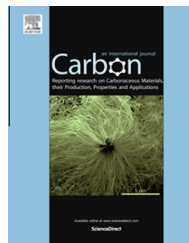




ELSEVIER

Available at www.sciencedirect.com

ScienceDirect

journal homepage: www.elsevier.com/locate/carbon

High surface area diamond-like carbon electrodes grown on vertically aligned carbon nanotubes

H. Zanin ^{a,b,*}, P.W. May ^a, R.L. Harniman ^a, T. Risbridger ^a, E.J. Corat ^b, D.J. Fermin ^{a,*}

^a School of Chemistry, University of Bristol, Cantocks Close, Bristol BS8 1TS, United Kingdom

^b National Institute for Space Research, Av. dos Astronautas 1758, São José dos Campos 12227-010, SP, Brazil

ARTICLE INFO

Article history:

Received 24 June 2014

Accepted 23 October 2014

Available online 30 October 2014

ABSTRACT

Electrochemically active diamond-like carbon (DLC) electrodes featuring high specific surface area have been prepared by plasma-enhanced chemical vapour deposition (CVD) onto densely packed forests of vertically aligned multiwall carbon nanotubes (VACNTs). The DLC:VACNT composite film exhibits a complex topography with web like features and ridges generated by partial coalescence of the DLC over the CNT arrays. DLC:VACNT electrodes exhibit low background responses over a large potential window, low uncompensated resistance, as well as low charge-transfer impedance in the presence of ferrocyanide as a redox probe. The interfacial capacitance associated with the DLC:VACNT electrode is in the range of 0.6 mF cm^{-2} , a value two orders of magnitude larger than in conventional flat carbon electrodes. DLC films grown onto single-crystal Si(100) under identical conditions resulted in essentially insulating layers. Conducting-atomic force microscopy studies reveal that the film electro-activity does not arise from specific topographic features in the highly corrugated film. The ensemble of experimental results suggests that the enhanced electrochemical responses are not connected to areas in which the CNT support is exposed to the electrolyte solution. This is remarkable behaviour considering that no dopants have been included during the DLC film growth.

© 2014 Elsevier Ltd. All rights reserved.

1. Introduction

Diamond-like carbon (DLC) is an interesting metastable form of amorphous carbon [1] that contains a mixture of tetrahedral (sp^3) and trigonal (sp^2) carbon hybridisations in varying amounts depending on its deposition conditions. Although amorphous DLC can be deposited at low (<200 °C) substrate temperature [2,3], it exhibits many of the extreme properties of crystalline diamond [4]. Among those properties are chemical inertness, optical transparency, high mechanical hardness, low friction coefficient and very high electrical resistance [5–7]. The electrical conductivity of DLC can be

significantly affected by the introduction of dopants during the film growth [8–12]. For instance, Liu and co-workers have grown nitrogen-doped DLC electrodes featuring a wide potential window, low background current and high corrosion resistance [13,14]. Other type of dopants, including nickel and boron, also result in films with excellent electrochemical properties [15–17].

An alternative approach to improving the conducting properties of DLC materials involves the incorporation of carbon nanotubes (CNTs). The effects of CNT content on internal stress, hardness and elasticity of DLC have already been considered in several reports [18–21]. Kinoshita et al. described an

* Corresponding authors at: School of Chemistry, University of Bristol, Cantocks Close, Bristol BS8 1TS, United Kingdom (H. Zanin).

E-mail addresses: hudson.zanin@bristol.ac.uk (H. Zanin), david.fermin@bristol.ac.uk (D.J. Fermin).

interesting approach to creating high surface area DLC structures via microwave plasma chemical vapour deposition (MPCVD) growth onto vertically aligned carbon nanotube (VACNT) arrays featuring number densities $1\text{--}7 \times 10^9 \text{ cm}^{-2}$ [22]. Recently, Zanin and co-workers developed a similar approach to prepare high surface area DLC electrodes showing excellent field emission properties [23]. Different DLC-coated CNT microstructures such as ‘teepees’, elongated ridges or ‘honeycombs’ were fabricated by tuning parameters such as the VACNT number density and DLC deposition conditions.

In the present work, we show for the first time that highly corrugated DLC films grown on VACNTs exhibit high electroactivity without the introduction of additional dopants. The as-grown DLC on VACNT (DLC:VACNT) were characterised by reversible electrochemical responses in the presence of ferrocyanide, with double layer capacitance larger than 0.6 mF cm^{-2} . DLC films grown on Si (100) wafers (DLC:Si) under identical conditions yielded inherently insulating layers. Conducting atomic force microscopy (AFM) measurements confirmed that the electroactivity of DLC:VACNT is not linked to specific topographic features in the highly corrugated films, with large portions of the surface exhibiting similar conductance values.

2. Experimental

2.1. Preparation of VACNT films

VACNT films were produced using a microwave plasma (MP) CVD chamber operating at 2.45 GHz [24]. Substrates were Ti sheets ($10 \text{ mm} \times 10 \text{ mm} \times 0.5 \text{ mm}$) covered with a 10 nm Ni layer deposited by electron-beam evaporation. The Ni layer was heated from 350 to 800°C over a period of 5 min in a N_2/H_2 ($10/90 \text{ sccm}$) plasma, inducing the formation of nanoparticles which promote the CNT growth. VACNT growth was initiated by introducing CH_4 (14 sccm) into the chamber for 1 min , maintaining a substrate temperature of 800°C and a reactor pressure of 30 torr . After growth, the sample was placed in a plasma enhanced chemical vapour deposition (PECVD) reactor (-400 V , pulse frequency 20 kHz) with an oxygen flow rate of 1 sccm at a pressure of 5 mtorr for 1 min . This was done in order to improve wettability and create oxygen-functional groups on the VACNT surfaces [25].

2.2. DLC film growth

DLC layers were deposited using a PECVD reactor fed with hexane vapour and argon gas at $0.1\text{--}0.3 \text{ torr}$ and a discharge voltage of -700 V at a pulse frequency of 20 kHz . For preparation of the composite DLC:VACNT samples, the previously prepared VACNT forest samples were used as substrates. Before growth, *n*-hexane was sprayed onto the samples and then the plasma was struck under argon and *n*-hexane vapour for 10 min [23].

Flat DLC electrodes were deposited onto a polished silicon (100) substrate for use as control samples. To prepare these, a Si wafer was placed into the PECVD reactor and cleaned using an argon plasma atmosphere at 0.1 torr (Ar flow rate of 1 sccm)

for 30 min . Next, *n*-hexane was sprayed into the active plasma region via a nozzle which directed downwards onto the substrate surface for 1 h for $1 \mu\text{m}$ DLC deposition, with Ar flowing during the whole process. After deposition, the DLC:Si samples were cooled down in high vacuum (10^{-6} torr) for 3 h [26].

2.3. Instrumentation and chemicals

DLC samples were characterised by high-resolution scanning electron microscopy (HR-SEM), Raman spectroscopy, tunnelling AFM and electrochemical tests. HR-SEM was performed with a FEI Inspect F50 operated at $20\text{--}30 \text{ kV}$. Raman spectra were recorded at room temperature using a Renishaw microscope, employing argon-ion laser excitation ($\lambda = 514.5 \text{ nm}$) with a laser power of $\sim 6 \text{ mW}$ and a spot size $\sim 15 \mu\text{m}$. Curve fitting and data analysis Fitlyk software was used to assigned the peak locations and fit all spectra. The tunnelling AFM measurements were performed with a Bruker Multimode with Nanoscope V controller with Picoforce Extender.

Cyclic voltammetry (CV) and electrochemical impedance spectroscopy (EIS) were recorded with an Autolab PGSTAT30 potentiostat. The electrochemical responses of DLC grown on either Si or VACNT were measured in Ar-saturated aqueous electrolyte solutions containing KNO_3 and $\text{K}_4\text{Fe}(\text{CN})_6$ as the supporting electrolyte and redox probe, respectively. The geometrical surface area of the working electrode was defined by using chemically-inert adhesive 3M Teflon tape to mask off some of the film, leaving a 3-mm-diameter open hole of fixed area (0.071 cm^2). The electrical contact was made on the top of the electrode using silver paste and copper wire. Ag/AgCl (in saturated KCl) and a pure platinum mesh were employed as reference and counter electrodes, respectively. All chemicals and electrodes were purchased from Sigma Aldrich.

3. Results and discussion

3.1. Structural characterisation of the DLC layers

The morphologies of DLC:Si, VACNT and DLC:VACNT films as imaged by SEM are shown in Fig. 1. DLC films directly grown on Si wafer are featureless on the micrometre scale, as illustrated in Fig. 1(a). The as-grown VACNT array shown in Fig. 1(b) reveals a high degree of nanotube alignment in a very close-packed configuration. Individual CNTs are, on average, $40 \mu\text{m}$ long with a cross sectional diameter of $\sim 60 \text{ nm}$. In contrast to the featureless DLC:Si films, the DLC:VACNT films are highly corrugated, as seen by the top view shown in Fig. 1(c). It seems that DLC deposition caused the tips of the CNTs to clump together to form a microstructured surface with ridges (Fig. 1(d)) and valleys (Fig. 1(e) and (f)). As discussed below, AFM analysis shows that the characteristic height of the ridges is $\sim 20 \mu\text{m}$. These results suggest that the high-lying areas are dense agglomerated packets of aligned nanotubes, forming a wide U-shaped valley due to the CNTs joining together. Fig. 1(d) indicates that after a few minutes of DLC deposition, the VACNT tips have become stuck together, and have been completely covered by DLC. In the valleys, a network of DLC-covered nanotubes is observed, and there is no evidence of exposed substrate. Fig. 1(f) shows the smallest

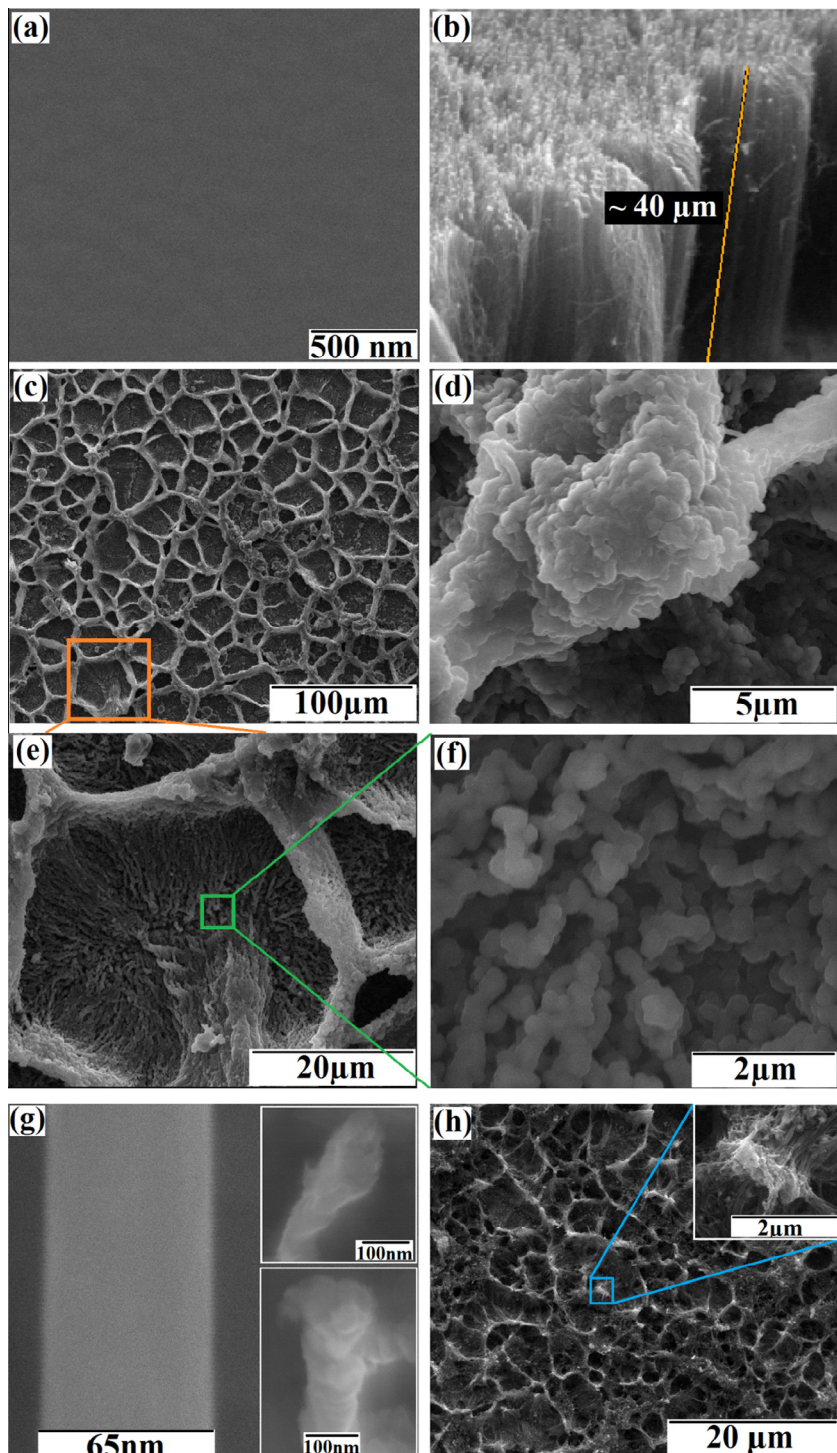


Fig. 1 – Electron microscope images of the sample morphologies: (a) DLC:Si film; (b) the as-grown VACNT forest; (c) Top view of the DLC:VACNT composite showing web-like structures; (d–f) higher magnification images of the DLC coating on top of the VACNT forest, showing the convoluted structure of the ridges and valleys; (g) as-grown single CNT and (inset) a single CNT coated by DLC film, allowing an estimate of the DLC thickness; (h) water-wetted VACNT sample, showing microstructure formation. (A colour version of this figure can be viewed online.)

features observed in the valley regions, although no particular topographic features can be assigned to the underlying nanotube array. Fig. 1(g) contrasts the image of an as-grown single CNT with a diameter ~ 65 nm with a single DLC-covered CNT,

showing cross-sections of 100–120 nm (inset in Fig. 1(g)), which suggests that the DLC thickness on the CNT walls is ~ 25 nm. For comparison, Fig. 1(h) shows an image of a VACNT forest electrode after wetting with a drop of water and drying

at room temperature. The water causes the CNT tips to stick together, forming a microstructure similar to that showed in Fig. 1(c). These structures are formed as surface tension forces on the wet CNT pulled them together. Even after water has evaporated away, the CNTs remain weakly bonded by van der Waals forces. The similarity of these to the structures in Fig. 1(c) suggests that DLC deposition acts in a similar way, sticking the CNTs together by the surface tension of hexane vapour used for the DLC growth.

Fig. 2 contrasts the Raman spectra of DLC films grown on VACNTs and on the Si wafer, as well as the as-grown VACNT array. The spectrum of the DLC:Si film (Fig. 2(b)) exhibits two broad bands centred at 1340 cm^{-1} (D-band) and 1537 cm^{-1} (G-band), arising from breathing and stretching vibrational modes of sp^2 carbon sites, respectively [23,27,28]. The spectrum from the as-grown VACNT arrays (Fig. 2(c)) can be deconvoluted into five distinct bands, including the sharp D and G-bands at 1357 and 1585 cm^{-1} , respectively. The D-band for CNTs is related to defects and disordered carbon whilst the G-band (E_{2g}) is related to well-ordered crystalline graphite [29]. Other modes include the so-called D'-band (1622 cm^{-1}) commonly associated with disordered carbon structures [25], the band at 1230 cm^{-1} attributed to various vibrational modes close to the K point, and the 1480 cm^{-1} band linked to nano-

sized carbon or trans-polyacetylene [31]. The Raman spectrum of the DLC:VACNT sample (Fig. 2(d)) appears as a combination of the DLC and VACNT Raman characteristics [26]. These observations suggest that the integrity of the individual CNTs is not affected by the subsequent DLC growth [23].

The presence of hydrogen in the PECVD process ensures that H will be incorporated in these DLC films, meaning, strictly speaking, they should be described as hydrogenated amorphous carbon films (a-C:H). The hydrogen atoms are mainly bonded to olefinic groups leading to a high content of sp^3 carbon in the DLC film, probably in the form of pendant CH_2 or CH_3 groups [30]. Based on the analysis reported by Ferrari et al. [31] the Raman intensity ratio I_D/I_G can be used to estimate the sp^3 carbon content and the optical band gap [32,33]. In the case of the DLC:Si film, the observed ratio $I_D/I_G = 0.28$ is consistent with an sp^3 carbon content of 60–70% and an optical band gap of 2.0–2.5 eV. For the DLC:VACNT film $I_D/I_G = 0.52$, which corresponds to 45–55% sp^3 carbon and a smaller band gap of between 1.6 and 1.8 eV.

3.2. Electrochemical properties of DLC:VACNT films

Cyclic voltammograms (CVs) of DLC:Si, VACNT and DLC:VACNT film electrodes in 0.1 M KNO_3 electrolyte solution scanned

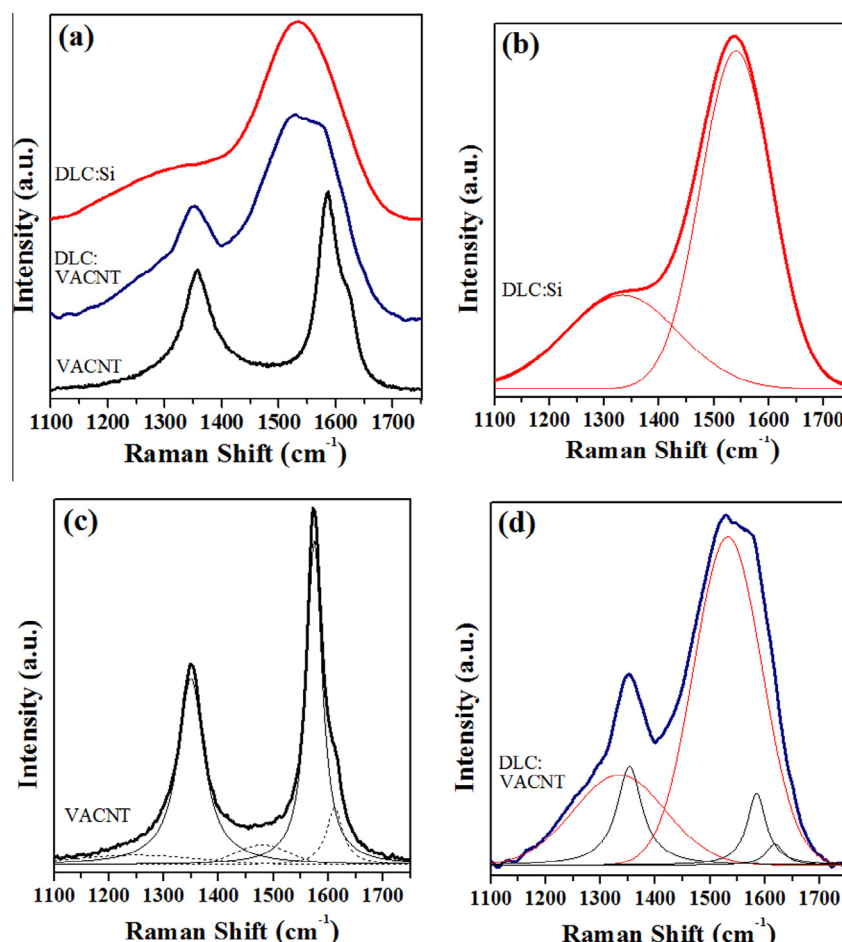


Fig. 2 – (a) Raman spectra of DLC:Si, DLC:VACNT and VACNT samples. The Raman spectra for (b) DLC:Si, (c) VACNT and (d) DLC:VACNT are deconvoluted as described in the main text. (A colour version of this figure can be viewed online.)

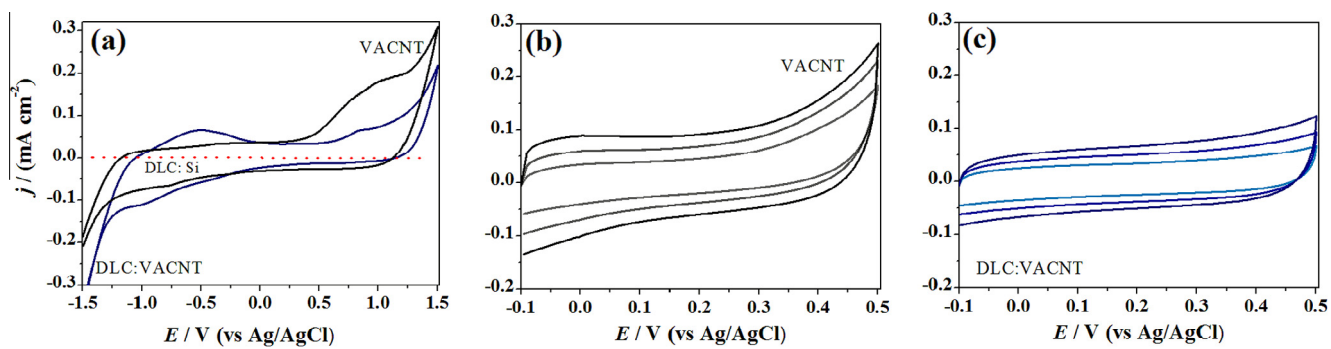


Fig. 3 – (a) Cyclic voltammograms from DLC:Si, VACNT and DLC:VACNT electrodes (electrode surface area 0.07 cm^2) taken at 100 mV s^{-1} in 0.1 M KNO_3 . The CV from DLC:Si is shown as a dotted red horizontal line due to its insulating nature. Cyclic voltammetry from (b) VACNT and (c) DLC-coated VACNT electrodes in 0.1 M KNO_3 taken at different scan rates from 50, 75 and 100 mV s^{-1} . (A colour version of this figure can be viewed online.)

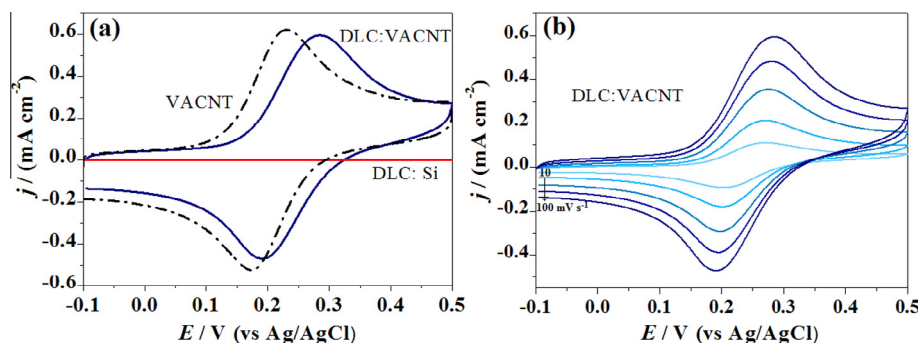


Fig. 4 – (a) Comparison of CV curves of 1 mM potassium ferrocyanide in 0.1 M potassium nitrate for DLC:Si, VACNT and DLC:VACNT electrodes (electrode surface area 0.07 cm^2) taken at a constant 100 mV s^{-1} scan rate. (b) CV responses obtained using DLC-coated VACNT electrodes in 1 mM potassium ferrocyanide in 0.1 M potassium nitrate taken at different scan rates ($10, 25, 50, 75, 100 \text{ mV s}^{-1}$). (A colour version of this figure can be viewed online.)

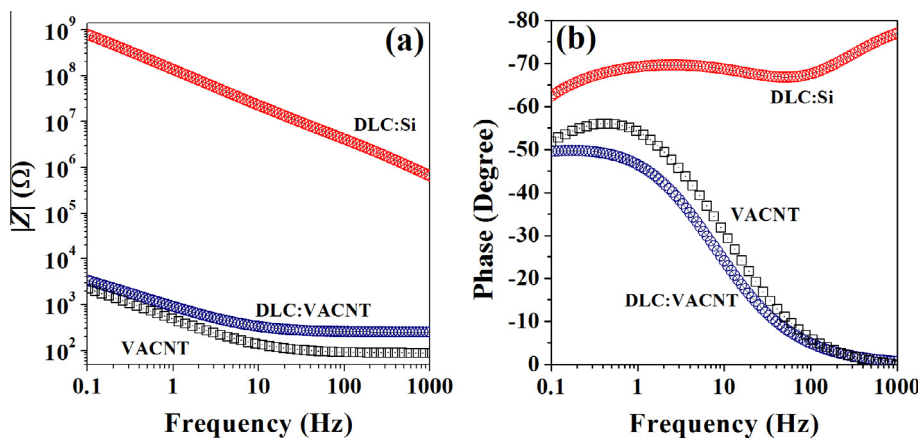


Fig. 5 – Impedance spectra taken at the formal redox potential of the ferro/ferricyanide couple for DLC:Si, VACNT and DLC:VACNT electrodes. The electrolyte contains 1 mM potassium ferrocyanide with 0.1 M potassium nitrate aqueous solution. The data are presented as Bode plots: (a) the modulus of the impedance amplitude $|Z|$, and (b) the phase of the impedance response versus the frequency. (A colour version of this figure can be viewed online.)

at 100 mV s^{-1} are displayed in Fig. 3(a). There is a remarkable contrast between the background current observed for the DLC films on Si with respect to those on VACNT. The

DLC:VACNT electrode exhibits capacitive currents comparable to those obtained for the VACNT films, with a similar potential window. A broadening of the capacitive current for

VACNT films at potentials above 0.3 V is consistent with the formation of oxygenated groups at the surface of the nanotubes. This response is significantly suppressed in the case of DLC:VACNT. In the case of DLC:Si, the film effectively behaves as a highly insulating layer. This behaviour is consistent with conventional DLC films grown in the absence of doping elements [4,26,34].

Fig. 3(b and c) displays the CVs of (b) VACNT and (c) DLC:VACNT electrodes as a function of the potential scan rate. The potential range was narrowed down in order to avoid interferences from the Faradaic responses associated with the oxygenated surface functional groups. The capacitive current increases linearly with the potential scan rate, resulting in a differential capacitance of 875 and $642 \mu\text{F cm}^{-2}$ for (b) VACNT and (c) DLC:VACNT at 0.15 V. Considering that typical double-layer capacitance values for carbon electrodes are of the order of $5 \mu\text{F cm}^{-2}$ [35], it can be estimated that the roughness factor associated with the DLC:VACNT electrode is approximately 130. If we consider a similar specific capacitance for VACNT and DLC:VACNT, this result suggests that the DLC growth leads to a $32 \pm 4\%$ decrease in the electroactive surface area. This observation appears consistent with the CNT bundling induced by the DLC growth. However, it should also be considered that other parameters can also play a role in changes of the double-layer capacitance in these highly porous assemblies, such as surface wettability and the penetration of the electrolyte solution.

Characteristic voltammograms for the various carbon electrodes in the presence of $1 \times 10^{-3} \text{ mol dm}^{-3} \text{ K}_4\text{Fe}(\text{CN})_6$ at 100 mV s^{-1} are shown in **Fig. 4(a)**. While VACNT and DLC:VACNT electrodes show well-defined redox responses, no clear faradaic signals are observed for DLC:Si films. An interesting observation is the slight offset in the potential of the redox responses for the VACNT electrode with respect to the DLC:VACNT electrode. This is associated with generation of Donnan potentials with the highly porous carbon nanotube arrays. These phenomena will be investigated in more detail in a separate communication. In the case of DLC:VACNT, a high degree of reversibility is observed at various scan rates, as shown in **Fig. 4(b)**. The peak currents are proportional to the square root of the scan rate, which allow estimating a diffusion coefficient of the redox probe of $7 \times 10^{-6} \text{ cm}^2 \text{ s}^{-1}$ based on Randles–Sevcik equation [36].

Further evidence of the electroactive nature of the DLC film grown on VACNT arrays is illustrated by the electrochemical impedance spectra shown in **Fig. 5**. The magnitude of the impedance amplitude ($|Z|$) is several orders higher for the DLC:Si film than for the DLC:VACNT film. The growth of DLC leads to an increase of $|Z|$ with respect to that from VACNT. The frequency dependence of the amplitude and phase is compatible with a conventional Randles model in the case of DLC:VACNT and VACNT over significant portions of the frequency range. In contrast, DLC:Si is characterised by quasi-capacitive behaviour over the entire frequency range. The DLC:VACNT spectra has been fitted to the Randles model down to frequencies of 1 Hz. The impedance analysis resulted

in values for uncompensated resistance of $216 \pm 6 \Omega$, a Warburg element (Y_0) of $0.22 \text{ m s}^{0.5} \Omega^{-1}$ (consistent with the diffusion coefficient of the redox probe) and capacitance from double layer formation of $(45 \pm 3) \times 10^{-6} \text{ F}$.

At frequencies below 1 Hz, the diffusion kinetics within the porous nature of the electrodes can be probed. This behaviour is determined by the phase angle above the 45° limit expected for planar diffusion. This trend is more pronounced in the case of the VACNT electrode indicating that the thin DLC layer decreases the porosity of the DLC to a certain extent. In order to fully describe the impedance responses over the entire potential range, more complex equivalent circuits should be used, incorporating transmission lines. For the purpose of this work, we shall limit our analysis to frequencies above 1 Hz. In a subsequent publication, we shall describe a more complete analysis allowing quantification of the penetration of the electrolyte within the porous VACNT structure.

The electrochemical responses of the DLC:VACNT films provide evidence that the films are conducting over the whole surface. This is a remarkable result considering the essentially insulating nature of the DLC films grown on Si substrates under identical conditions. Although evidence based on the differential capacitance and the impedance spectra indicate that the whole film is electroactive, it could be argued that the electron transfer only takes place at discrete sites in which nanotubes are exposed to the electrolyte. In the next section, we shall discuss this issue further.

3.3. Conductance Mapping of VACNT:DLC films

In order to determine whether the convoluted topology of the DLC:VACNT film influenced its electroactivity, conducting AFM was used to simultaneously map the height of a surface ridge along with its conductivity (**Fig. 6**). A $30 \mu\text{m}$ line scan was performed which measured the height (z) of the ridge from its peak ($z = 19 \mu\text{m}$) to the valley bottom ($z = 0 \mu\text{m}$), as shown in **Fig. 6(a)**. Regions marked in green ($0\text{--}2 \mu\text{m}$), blue ($13\text{--}15 \mu\text{m}$) and red ($28\text{--}30 \mu\text{m}$) correspond to the top, middle and bottom of the ridge, respectively. **Fig. 6(b)** shows the root-mean-square (RMS) of the current response obtained from a number of $2 \mu\text{m} \times 2 \mu\text{m}$ regions spanning the $30 \mu\text{m}$ line scan. The data show that the RMS current at the top of the ridges has a very similar value to that from the low-lying areas of the film, and that the measured current (and hence film conductivity) is independent of topology.

Fig. 6(c-h) show a series of $2 \mu\text{m} \times 2 \mu\text{m}$ topographic images of a DLC:VACNT film alongside the corresponding current maps for the top, middle and bottom areas of the ridge. Although contrast in conductance is observed between grains and grain boundaries [37], there is no clear correlation with larger scale topographic features. These results suggest that the origin of the DLC:VACNT electroactivity is connected to areas of high electron density at the surface rather than to portions of the nanotube support directly exposed to the electrolyte solution.

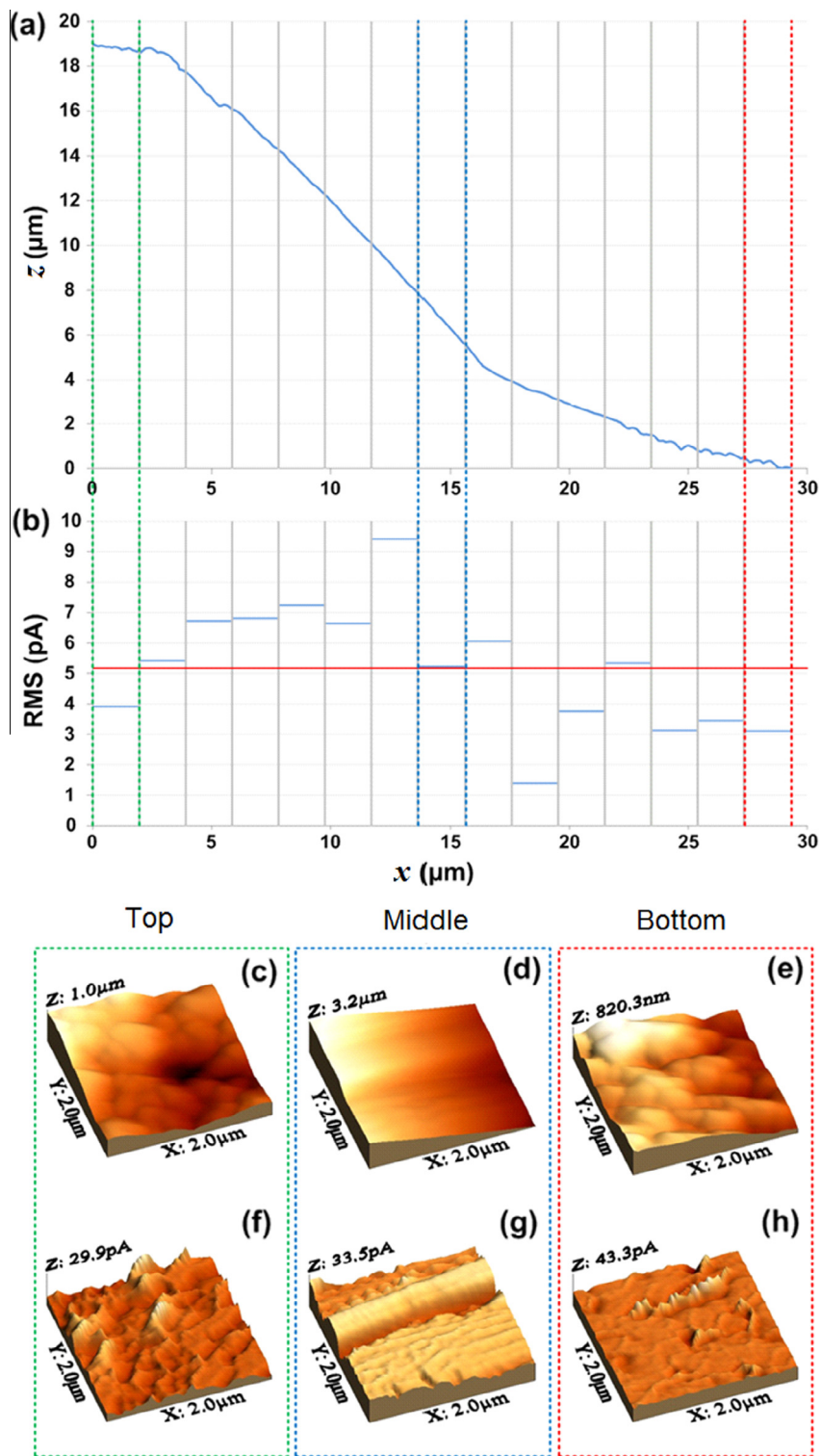


Fig. 6 – Conducting AFM measurements of the topography and current taken over a $2 \times 30 \mu\text{m}$ scan region extending from the base to the peak of a ridge structure in a DLC:VACNT film. $2 \times 2 \mu\text{m}$ scans were collected incrementally with an applied tip-sample bias of 100 mV. (a) Topographic data for the central line of each $2 \times 2 \mu\text{m}$ scan combined to produce a single continuous line scan, displayed as vertical height, z , over a height of 19 μm . Regions defined as the ‘top’, ‘middle’ and ‘bottom’ of the ridge are outlined using green, blue and red dashed lines, respectively. (b) Total RMS current measured across each $2 \times 2 \mu\text{m}$ scan; the red line at 5.2 pA represents the average current across the whole $2 \times 30 \mu\text{m}$ region with an average RMS error of 39%. The lower 6 images are three-dimensional representations of the topography and current measured at the three different positions on the ridge: (c and f) top of the ridge (green dashed lines), (d and g) middle of the ridge (blue dashed lines), (e and h) base of the ridge (red dashed lines). (A colour version of this figure can be viewed online.)

4. Conclusions

The present work demonstrates for the first time that electroactive DLC films can be grown on VACNT arrays by PECVD without the introduction of dopants. Such highly corrugated DLC:VACNT films show web-like structures and ridges across the surface, and behave as conducting, high-surface-area, robust, all-carbon electrodes. The topography and electroactivity of DLC:VACNT films are in stark contrast with the smooth and insulating characteristics of DLC films grown on Si wafers under identical conditions. Cyclic voltammetry and impedance spectroscopy in the presence of ferrocyanide as a redox probe exhibit reversible behaviour with a differential capacitance above 0.6 mF cm^{-2} . Analysis of the topographic and conductance images demonstrated that the film electroactivity is not linked to specific topographic features. SEM data show that the DLC thickness is $\sim 25 \text{ nm}$, excluding the possibility of direct tunnelling of electrons across this DLC layer. It could be argued that electronic states in the CNT arrays overlap with the electronic bands of the DLC layer, creating a quasi-degenerate DLC film. This would be consistent with the Raman measurements which showed that the DLC:VACNT films had a reduced band gap compared to DLC alone. To further advance our understanding of this complex composite material, high resolution mapping of electrochemical activity should be recorded. In this sense, novel approaches such as Scanning Electrochemical Cell microscopy would be very valuable [38].

Acknowledgements

The electron microscopy work was performed with JEOL 6330 microscope at University of Bristol and with a HRSEM (FEI-Inspect) microscope at the LME/LNLS-Campinas. We also gratefully acknowledge CNPq (202439/2012-7), Fapesp (2014/02163-7) and EPSRC (EP/K007025/1) for financial support.

REFERENCES

- [1] Robertson J. Diamond-like amorphous carbon. Materials Science & Engineering R-Reports. 2002;37(4–6):129–281.
- [2] Bewilogua K, Cooper CV, Specht C, Schroder J, Wittorf R, Grischke M. Effect of target material on deposition and properties of metal-containing DLC (Me-DLC) coatings (vol 127, pg 224, 2000). Surf Coat Technol 2000;132(2–3):275–83.
- [3] de Castro Costa RP, Marciano FR, Lima Oliveira DA, Travai-Airoldi VJ. Enhanced DLC wear performance by the presence of lubricant additives. Materials Research-Ibero-American. J Mater 2011;14(2):222–6.
- [4] Zeng A, Neto VF, Gracio JJ, Fan QH. Diamond-like carbon (DLC) films as electrochemical electrodes. Diam Relat Mater 2014;43:12–22.
- [5] Omer AMM, Adhikari S, Adhikary S, Rusop M, Uchida H, Soga T, et al. Electrical conductivity improvement by iodine doping for diamond-like carbon thin-films deposited by microwave surface wave plasma CVD. Diam Relat Mater 2006;15(4–8):645–8.
- [6] Adhikary S, Tian XM, Adhikari S, Omer AMM, Uchida H, Umeno M. Bonding defects and optical band gaps of DLC films deposited by microwave surface-wave plasma CVD. Diam Relat Mater 2005;14(11–12):1832–4.
- [7] Choi J, Nakao S, Kim J, Ikeyama M, Kato T. Corrosion protection of DLC coatings on magnesium alloy. Diam Relat Mater 2007;16(4–7):1361–4.
- [8] Chen CW, Robertson J. Doping mechanism in tetrahedral amorphous carbon. Carbon 1999;37(5):839–42.
- [9] Compton RG, Foord JS, Marken F. Electroanalysis at diamond-like and doped-diamond electrodes. Electroanalysis 2003;15(17):1349–63.
- [10] Hayashi Y, Ishikawa S, Soga T, Umeno M, Jimbo I. Photovoltaic characteristics of boron-doped hydrogenated amorphous carbon on n-Si substrate prepared by rf plasma-enhanced CVD using trimethylboron. Diam Relat Mater 2003;12(3–7):687–90.
- [11] Rusop M, Mominuzzaman SM, Soga T, Jimbo T, Umeno M. Characterization of phosphorus-doped amorphous carbon and construction of n-carbon/p-silicon heterojunction solar cells. Jpn J Appl Phys 2003;42(4B):2339–44.
- [12] Veerasamy VS, Amaralunga GAJ, Davis CA, Timbs AE, Milne WI, McKenzie DR. N-type doping of highly tetrahedral diamond-like amorphous-carbon. J Phys 1993;5(13):L169–74.
- [13] Liu LX, Liu E. Nitrogenated diamond-like carbon films for metal tracing. Surf Coat Technol 2005;198(1–3):189–93.
- [14] Liu E, Kwek HW. Electrochemical performance of diamond-like carbon thin films. Thin Solid Films 2008;516(16):5201–5.
- [15] Maalouf R, Chebib H, Saikali Y, Vittori O, Sigaud M, Garrelie F, et al. Characterization of different diamond-like carbon electrodes for biosensor design. Talanta 2007;72(1):310–4.
- [16] Kim J-I, Bordeanu A, Pyun J-C. Diamond-like carbon (DLC) microelectrode for electrochemical ELISA. Biosens Bioelectron 2009;24(5):1394–8.
- [17] Schnupp R, Kuhnhold R, Temmel G, Burte E, Ryssel H. Thin carbon films as electrodes for bioelectronic applications. Biosens Bioelectron 1998;13(7–8):889–94.
- [18] Hu H, Chen G, Zha J. Facile synthesis of CNTs-doped diamond-like carbon film by electrodeposition. Surf Coat Technol 2008;202(24):5943–6.
- [19] Wei C, Wang C-I, Tai F-C, Ting K, Chang R-C. The effect of CNT content on the surface and mechanical properties of CNTs doped diamond like carbon films. Diam Relat Mater 2010;19(5–6):562–6.
- [20] Kinoshita H, Ippei I, Sakai H, Ohmae N. Synthesis and mechanical properties carbon nanotube/diamond-like carbon composite films. Diam Relat Mater 2007;16(11):1940–4.
- [21] Wei C, Yang J-F. A finite element study on the hardness of carbon nanotubes-doped diamond-like carbon film. J Mater Res 2012;27(1):330–8.
- [22] Kinoshita H, Ippei I, Sakai H, Ohmae N. Synthesis and mechanical properties carbon nanotube/diamond-like carbon composite films. Diam Relat Mater 2007;11:1940–4.
- [23] Zanin H, May PW, Hamanaka MHMO, Corat EJ. Field emission from hybrid diamond-like carbon and carbon nanotube composite structures. ACS Appl Mater Interf 2013;5(23):12238–43.
- [24] Zanin H, May PW, Fermin DJ, Plana D, Vieira SMC, Milne WI, et al. Porous boron-doped diamond/carbon nanotube electrodes ACS. Acs Appl Mater Interf 2014;6(2):990–5.
- [25] Lobo AO, Ramos SC, Antunes EF, Marciano FR, Travai-Airoldi VJ, Corat EJ. Fast functionalization of vertically aligned multiwalled carbon nanotubes using oxygen plasma. Mater Lett 2012;70:89–93.
- [26] Zanin HG, May PW, Lobo AO, Saito E, Machado JPB, Martins G, et al. J Electrochem Soc 2014;161(5):H290–5.

- [27] Ferrari AC, Robertson J. Interpretation of Raman spectra of disordered and amorphous carbon. *Phys Rev B* 2000;61:14 095–107.
- [28] Zanin H, Margraf-Ferreira A, da Silva NS, Marciano FR, Corat EJ, Lobo AO. Graphene and carbon nanotube composite enabling a new prospective treatment for trichomoniasis disease. *Mater Sci Eng C* 2014;41:65–9.
- [29] Zanin H, Saito E, Marciano FR, Ceragioli HJ, Granato AEC, Porcionatto M, Lobo AO. Fast preparation of nano-hydroxyapatite/superhydrophilic reduced graphene oxide composites for bioactive applications. *J Mater Chem B* 2013;1(38):4947–55.
- [30] Irmer G, Dorner-Reisel A. Micro-Raman studies on DLC coatings. *Adv Eng Mater* 2005;7(8):694–705.
- [31] Ferrari AC, Robertson J. Raman spectroscopy of amorphous, nanostructured, diamond-like carbon, and nanodiamond. *Philos Transact R Soc 1824;2004(362):2477–512.*
- [32] Tamor MA, Vassell WC. Raman fingerprinting of amorphous-carbon films. *J Appl Phys* 1994;76(6):3823–30.
- [33] Ferrari AC, Robertson J. Interpretation of Raman spectra of disordered and amorphous carbon. *Phys Rev B* 2000;61(20).
- [34] Papakonstantinou P, Zhao JF, Lemoine P, McAdams ET, McLaughlin JA. The effects of Si incorporation on the electrochemical and nanomechanical properties of DLC thin films. *Diam Relat Mater* 2002;11(3–6):1074–80.
- [35] Bradbury CR, Kuster L, Fermín DJ. Electrochemical reactivity of HOPG electrodes modified by ultrathin films and two-dimensional arrays of metal nanoparticles. *J Electroanal Chem* 2010;646(1–2):114–23.
- [36] Silva TA, Zanin H, Saito E, Medeiros RA, Vicentini FC, Corat EJ, et al. Electrochemical behaviour of vertically aligned carbon nanotubes and graphene oxide nanocomposite as electrode material. *Electrochim Acta* 2014;119:114–9.
- [37] Chatterjee V, Harniman R, May PW, Barhai PK. Direct observation of electron emission from the grain boundaries of chemical vapour deposition diamond films by tunnelling atomic force microscopy. *Appl Phys Lett* 2014;104:171907.
- [38] Snowden ME, Güell AG, Lai SCS, McKelvey K, Ebejer N, O'Connell MA, et al. Scanning electrochemical cell microscopy: theory and experiment for quantitative high resolution spatially-resolved voltammetry and simultaneous ion-conductance measurements. *Anal Chem* 2012;84(5):2483–91.